Structural, electronic and magnetic properties of the Mn–Ni(110) $c(2\times2)$ surface alloy*

Li Deng-Feng(李登峰)[a)b)†], Xiao Hai-Yan(肖海燕)[b)], Zu Xiao-Tao(祖小涛)[b)],
Dong Hui-Ning(董会宁)[a)], and Gao Fei(高 飞)[c)]

[a)] *Department of Mathematics and Physics, Chongqing University of Posts and Telecommunications, Chongqing* 400065, *China*
[b)] *Department of Applied Physics, University of Electronic Science and Technology of China, Chengdu* 610054, *China*
[c)] *Pacific Northwest National Laboratory, P. O. Box* 999, *Richland, WA* 99352, *USA*

(Received 29 September 2009; revised manuscript received 8 February 2010)

Using first-principles total energy method, we study the structural, the electronic and the magnetic properties of the MnNi(110) $c(2\times2)$ surface alloy. Paramagnetic, ferromagnetic, and antiferromagnetic surfaces in the top layer and the second layer are considered. It turns out that the substitutional alloy in the outermost layer with ferromagnetic surface is the most stable in all cases. The buckling of the Mn–Ni(110) $c(2\times2)$ surface alloy in the top layer is as large as 0.26 Å (1 Å=0.1 nm) and the weak rippling is 0.038 Å in the third layer, in excellent agreement with experimental results. It is proved that the magnetism of Mn can stabilize this surface alloy. Electronic structures show a large magnetic splitting for the Mn atom, which is slightly higher than that of Mn–Ni(100) $c(2\times2)$ surface alloy (3.41 eV) due to the higher magnetic moment. A large magnetic moment for the Mn atom is predicted to be 3.81 $\mu_{\rm B}$. We suggest the ferromagnetic order of the Mn moments and the ferromagnetic coupling to the Ni substrate, which confirms the experimental results. The magnetism of Mn is identified as the driving force of the large buckling and the work-function change. The comparison with the other magnetic surface alloys is also presented and some trends are predicted.

Keywords: manganese, nickel, magnetic surface alloy, density of states, density functional theory

PACC: 7115M, 7120C, 7510

1. Introduction

The study of magnetically stabilized surface alloys has attracted considerable attention due to unusual magnetic phenomena in two-dimensional structures. Experimental and theoretical analyses showed that a class of magnetic alloys have highly corrugated surface. It was confirmed that the large rippling and the stabilities of magnetic alloys are correlated to the large magnetic moments of the adsorbates.[1−5] The Mn–Cu(100) $c(2\times2)$ surface alloy has been investigated by low energy electron diffraction (LEED), and an unusually large outward relaxation of the Mn atoms was observed. *Ab initio* calculations performed by Wuttig *et al.* demonstrated that the large buckling and stability of the magnetic alloy were derived from a large magnetic moment of 3.75 $\mu_{\rm B}$ per Mn atom.[6] O'Brien *et al.* also studied the Mn–Cu(100) $c(2\times2)$ and Mn–Ni(100) $c(2\times2)$ surface alloys by using the x-ray magnetic circular dichroism (XMCD) technique.[7] However, the long-range magnetic order of Mn was observed only for the Ni-based alloy from their results. It was suggested that only the large magnetic moment of Mn, which resulted in an increase in magnetic energy, stabilized these structures. Rader *et al.* also predicted that Mn–Ni(100) $c(2\times2)$ was a new magnetic surface alloy based on the detailed comparison with the Mn–Cu(100) $c(2\times2)$ case.[8,9] In their work the electronic structures were presented both experimentally and theoretically. The magnetic moment values of Mn atoms were measured to be 3.75 $\mu_{\rm B}$ and 3.5 $\mu_{\rm B}$ for Mn–Cu(100) $c(2\times2)$ and Mn–Ni(100) $c(2\times2)$ surfaces, respectively. A large magnetic splitting due to the localization of Mn–3d states was observed.

The Mn–Ni(110) $c(2\times2)$ surface alloy has also drawn much attention of the experimental research in recent years. Rader *et al.* predicted that this is a new magnetic surface alloy based on the detailed

*Project supported by the Special Funds of the National Natural Science Foundation of China (Grant No. 10947102), the Foundation of Education Committee of Chongqing, China (Grant No. KJ090503), the Foundation of Science Committee of Chongqing, China (Grant No. CSTC 2007BB4385), and the Doctoral Foundation of Chongqing University of Posts and Telecommunications, China (Grant No. A2008-64).
†Corresponding author. E-mail: lidf@cqupt.edu.cn
© 2010 Chinese Physical Society and IOP Publishing Ltd

comparison with the Mn–Cu(100) $c(2\times2)$ case.[9] The XMCD signal showed that there is a long-range magnetic ordering in the Mn submonolayer and its magnetic moment is parallel to that of the Ni substrate.[10] Surface x-ray diffraction technique was employed by Santis *et al.* to determine the structure of this surface phase.[11] The rippling of this surface alloy in the top layer was found to be 0.30±0.03 Å while this surface was suggested to be much smoother from a simple hard-sphere picture using the usual atomic (metallic) radii. Furthermore, no theoretical studies of the Mn–Ni(110) $c(2\times2)$ surface alloy by first-principles calculations have been reported.

In this work, we present an *ab initio* investigation of the structural, the electronic and the magnetic properties of Mn adsorption on the Ni(110) surface. The paramagnetic (PM), the ferromagnetic (FM) and the antiferromagnetic (AFM) surfaces are considered, and the structure of Mn–Ni(110) $c(2\times2)$ surface alloy is reproduced by our calculations. We explore the influence of magnetism for Mn atoms on the structural and the electronic properties. A comparison between our results and the results obtained from other magnetic surface alloys is also presented and some trends are predicted.

2. Computational approach

Ab initio total-energy calculations within the framework of density functional theory (DFT) by using VASP code were carried out in this study, where the electron–ion interaction was described by projector augmented wave (PAW) method.[12] All the calculations have been performed in the generalized gradient approximation (GGA) proposed by Perdew and Wang.[13,14] The electronic ground state was calculated with the residuum-minimization techniques, and the geometrical structure was optimized using the conjugated-gradient technique. The influence of different k-point samplings and plane-wave cutoff energies was explored in a series of test calculations. We used k-point grids of $8\times6\times1$ for the geometry optimization and $12\times10\times1$ for calculating the magnetic moments and the electronic structure at the equilibrium volume. The cutoff energy was set to be 350 eV. A five-layer slab of Ni, periodically repeated in a supercell geometry with seven equivalent layers of vacuum between any two successive metal slabs, was used. The bottom two layers of the slab were fixed at the bulk truncated positions, whereas all other atoms were allowed to relax. Adsorption was allowed on only one of the two exposed surfaces. In order to avoid the artificial macroscopic electrostatic field which arises from the inequivalence of the two sides of the slab, a planar dipole layer in the middle of the vacuum region as introduced by Neugebauer and Scheffler was considered.[15] During the structural optimization, we considered the PM, FM and AFM surfaces for Mn adsorption on the Ni(110) $c(2\times2)$ surface. For the case of FM and AFM surfaces, we investigated various combinations of FM and AFM coupling between Mn atoms, and between Mn and Ni atoms. The magnetic moment of the nearest neighbour atoms was set to be parallel or antiparallel to each other for the FM or AFM coupling respectively. The atomic sphere radii of Ni and Mn atoms were selected as 1.28 Å and 1.32 Å for all systems. The lattice parameter for Ni was calculated to be 3.515 Å in excellent agreement with an experimental value of 3.524 Å.

3. Results and discussion

3.1. Structural properties

Experimentally it has been found that the $c(2\times2)$ phase is stable with the deposition of about 0.5 monolayer (ML) coverage of Mn on Ni(110).[11] This is confirmed by our calculations that the adsorption energy of Ni(110) $c(2\times2)$–Mn surface is 0.88 eV lower than that of Ni(110) $p(2\times2)$–Mn surface. In this work, we took five different structural models into account: three high symmetry overlayer structures where Mn atoms occupy fourfold hollow sites (hol), long bridge sites (l-bri) and short bridge sites (s-bri) and two substitutional alloy models in the top layer (sub1) and in the subsurface layer (sub2) (see Fig. 1). In each case the PM, FM and AFM surfaces were considered.

In order to compare the stability of the substitutional adsorption with that of the on-surface adsorption it is necessary to define the adsorption energy per adatom. For on-surface adsorption, the adsorption energy per adatom is defined as[15]

$$E_{\rm ad} = (E_{\rm Mn/Ni-slab} - E_{\rm Ni-slab} - nE_{\rm Mn-atom})/n, \quad (1)$$

where $E_{\rm Ni-slab}$ and $E_{\rm Mn/Ni-slab}$ are the total energies of a clean Ni surface and the adsorbate system, respectively, n is the number of Mn atoms and $E_{\rm Mn-atom}$ is the total energy of a spin-polarized free Mn atom. In the case of Mn substitutional adsorption, a substrate atom is kicked out and moves to a kink site at a surface step, while an adsorbate atom moves to occupy the

vacancy. Thus, the adsorption energy for the surface-substitutional site can be defined as follows:[15]

$$E_{\rm ad}^{\rm sub} = \frac{1}{n}[E_{\rm Mn/Ni-slab}^{\rm sub} - (E^{\rm vac} + nE_{\rm Mn-atom}) + nE_{\rm f}^{\rm vac}], \quad (2)$$

and

$$E_{\rm f}^{\rm vac} = \frac{1}{n}(E^{\rm vac} + nE_{\rm bulk}^{\rm Ni} - E_{\rm Ni-slab}). \quad (3)$$

Here, $E_{\rm f}^{\rm vac}$ is the formation energy of a surface vacancy, $E^{\rm vac}$ is the total energy per unit cell of the surface with a vacancy, and $E_{\rm bulk}^{\rm Ni}$ is the total energy per atom of bulk fcc Ni. The surface vacancy formation energy of Ni(110) $c(2\times2)$ model was calculated to be 0.48 eV, smaller than that of the Ni(100) $c(2\times2)$ phase,[16] which indicates that the atoms of the Ni(110) $c(2\times2)$ model in the uppermost layer are more likely to be substituted. The vacancy formation energy of Ni(110) $c(2\times2)$ model in the second layer was calculated to be 1.04 eV.

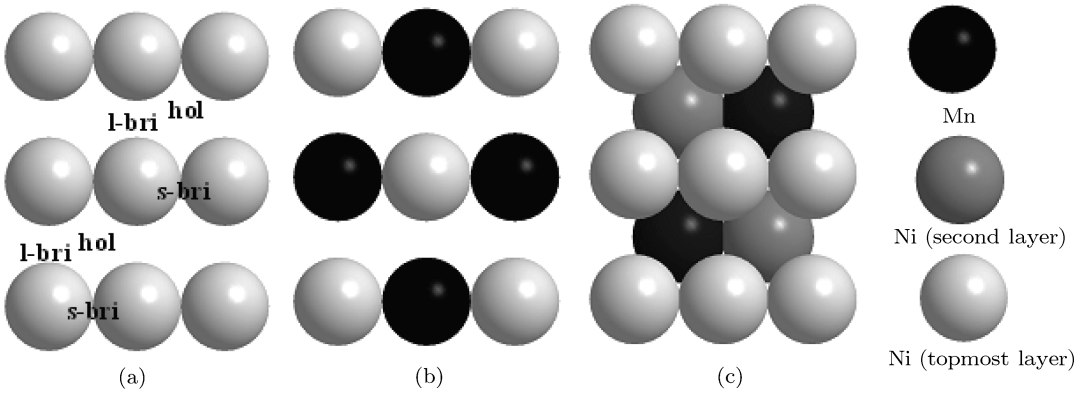


Fig. 1. Schematic plane view of the different adsorption sites for 0.5 ML Mn–Ni(110) $c(2\times2)$ surface. (a) Overlayer models including hollow (hol) sites, long bridge (l-bri) sites, short bridge (s-bri) sites; (b) substitutional sites with Mn atoms replacing top layer Ni atoms (Mn–Ni(110) $c(2\times2)$-sub1); (c) substitutional sites with Mn atoms replacing the second layer Ni atoms (Mn–Ni(110) $c(2\times2)$-sub2).

The calculated adsorption energies of all the structural models considered were given in Table 1. In the case of the AFM coupling for the substitutional adsorption, only the AFM coupling between the Mn adatoms for the $c(2\times2)$ phase was presented here since it is the most stable configuration under the condition of AFM coupling as suggested by the following research of magnetic properties. From Table 1, we can see that the substitutional site adsorption is always more favourable than other site adsorptions, and the surface alloys with FM and AFM surfaces are more stable than those with the PM surface. The most favourable structure is the ferromagnetic Mn/Ni substitutional alloy in the top layer, confirming the earlier experimental results.[9,11] The magnetic moment of the Mn atom was calculated to be 3.81 $\mu_{\rm B}$, larger than that of the Mn–Ni(100) $c(2\times2)$ surface alloy (3.5 $\mu_{\rm B}$).[8] Such an increase in the magnetic moment of the Ni (110)-based surface alloy may result from the fact that the fcc (110) surface is more open than (100) surface. In the case of on-surface adsorption, hollow site with AFM surface is preferred. The magnetic moments of two neighbouring Mn atoms are 3.97 $\mu_{\rm B}$ and –3.89 $\mu_{\rm B}$, higher than that for the substitutional geometry. It is indicated that a lower coordination and the missing nearest-neighbouring magnetic atoms may lead to a reduction in hybridization and an increase in magnetic moment.[17] In the FM and the AFM states, the surface alloy in the top layer is energetically preferred to the subsurface alloy, while the alloy in the subsurface layer is more stable in the PM state. This suggests that the stability of Mn/Ni alloy is affected by the magnetic moment of Mn atoms.

The optimized structural parameters are also listed in Table 1. For the surface alloy in the PM state, the Mn atoms move inward by 0.18 Å and locate below the Ni atoms in the same layer, whereas FM Mn atoms show a large outward buckling of 0.26 Å, similar to the case of Mn–Cu(110) $c(2\times2)$ surface alloy (inward buckling of 0.08 Å in the PM state and outward buckling of 0.16 Å in the FM state[17,18]). The large outward buckling of the FM surface is in accordance

with the experimental observation (0.30±0.03 Å).[11] The inward buckling for the PM surface is also consistent well with the classical point of view that smaller atoms should move inward upon adsorption. It is proved that the buckling can be attributed to the large magneto-volume effect of Mn atoms and the Mn–Ni(110) $c(2\times2)$ is a magnetic surface alloy, consistent with the case of Mn/Cu surface alloy.[17,19] The small buckling in the third layer was determined to be 0.038 Å as compared with the experimental result of 0.036±0.005 Å.[11] For the subsurface alloy in the PM state, nearly all the atoms remain at the ideal position with the exception of buckling of 0.12 Å in the second layer. The Mn–Ni nearest-neighbour (NN) distance of the Mn–Ni(110) $c(2\times2)$ surface alloy with the FM surface is calculated to be 2.5 Å, consistent well with the experimental value of 2.58±0.01 Å, and almost identical to that of the bulk $MnNi_3$ (2.54 Å).[20] It is interesting to find that for the surface alloy in the FM state there exists a large buckling in the top layer despite the fact that the NN distance is close to the $MnNi_3$ bulk value. It seems that the adsorption behaviour of Mn on Ni(110) $c(2\times2)$ surface is somewhat different from that on the Sn–Ni(110) $c(2\times2)$ surface alloy, which has a much smoother surface and shorter NN distance than the bulk Ni_3Sn.[16,21] Obviously the magnetic moments of Mn atoms have a considerable influence on surface geometrical structure. The interlayer distances are also presented in Table 1. For Mn–Ni(110) $c(2\times2)$ surface alloy with FM surface, we have observed an inward relaxation of the surface layer and an expansion of the second interlayer distance as compared with the ideal interlayer spacing of 1.24 Å for Ni(110). Our calculations are in excellent agreement with the experimental results.[11]

Table 1. Main energetic and structural properties for Mn adsorption on Ni(110) $c(2\times2)$ surface with different magnetic orientations. E_{ads} represents adsorption energy, ΔZ_i denotes the buckling of layer i, d_{ij} refers to the interlayer distance between layers i and j. Sub1, sub2, hol, l-bri, s-bri denote the Mn atom at the substitutional site in the top layer, the substitutional site in the second layer, hollow site, long bridge site, and short bridge site, respectively. The corresponding sites are presented in Fig. 1. Expt represents experimental results, FM stands for ferromagnetic, AFM for antiferromagnetic, and PM for paramagnetic.

		E_{ads}/eV	ΔZ_1/Å	ΔZ_2/Å	ΔZ_3/Å	d_{12}/Å	d_{23}/Å	d_{34}/Å	μ_{Mn}/μ_B	μ_{Ni}/μ_B
FM	sub1	–7.63	0.26		0.038	1.19	1.31	1.22	3.81	0.64
	sub2	–7.51		0.002		1.14	1.33	1.21	3.24	0.64
	hol	–6.95			0.11	0.88	1.29	1.28	3.51	0.42
	l-bri	–6.91				1.05	1.27	1.27	3.84	0.58
	s-bri	–5.79				1.88	1.11	1.33	4.03	0.60
AFM	sub1	–7.52	0.22		0.03	1.17	1.32	1.22	3.79, –3.88	0.52, 0.29
	sub2	–7.34		0.01		1.12	1.33	1.21	3.19, –3.13	0.36, 0.28
	hol	–7.18			0.09	1.21	1.19	1.31	3.97, –3.89	0.34
	l-bri	–6.81			0.02	1.02	1.29	1.26	3.84, –3.92	0.07, 0.54
	s-bri	–5.73				1.11	1.33	1.20	4.03, –4.12	0.59
PM	sub1	–6.63	–0.18		0.02	1.00	1.37	1.21		
	sub2	–7.04		0.12		1.11	1.28	1.21		
	hol	–5.83			0.14	0.83	1.32	1.26		
	l-bri	–6.01			0.28	0.43	1.48	1.23		
	s-bri	–3.76				1.10	1.33	1.22		
Expt[11]	sub1		0.30±0.3		0.036±0.05	1.28±0.2	1.254±0.05	1.242±0.05		

3.2. Electronic properties

On the basis of optimized structures, we also investigated electronic properties of a number of representative configurations. For Mn–Ni(110) $c(2\times2)$ surface alloy with the FM surface, the spin-split local density of states (LDOS) of Mn is shown in Fig. 2(a). The LDOS distribution shows a similar character to that of Mn–Ni(100) $c(2\times2)$ system.[22] The central peak of the minority Mn bands locates at 1.78 eV and the exchange splitting between majority and minority spin states is slightly larger than that of Mn–Ni(100) $c(2\times2)$ surface alloy (3.41 eV).[8] The larger magnetic exchange splitting is derived from the localization of Mn–3d states and higher

magnetic moments of the Mn atoms. This is consistent with the results obtained from the previous section. The broad majority-spin density of states indicates that there exists a strong hybridization between the 3d states of Mn and Ni. In the case of majority-spin LDOS, the DOS peaks exist at 1.31 eV and 1.85 eV that correspond to a small DOS distribution near the Fermi level. This is different from the case of Mn–Ni(100) $c(2\times2)$ surface alloy.[8] Figure 2(b) shows the LDOS obtained for the substrate atoms. It can be clearly seen that no characteristic sharp maximum is observed from the minority spins of the Ni–3d bands, which may result from the reduction of the Ni magnetic moments. The extended energy range of Ni–3d bands almost overlaps with that of Mn–3d bands, indicating the strong interaction between them. This is in agreement with the results from large transfer integrals that describe the hybridization between Mn 3d and Ni 3d states as previously reported.[9]

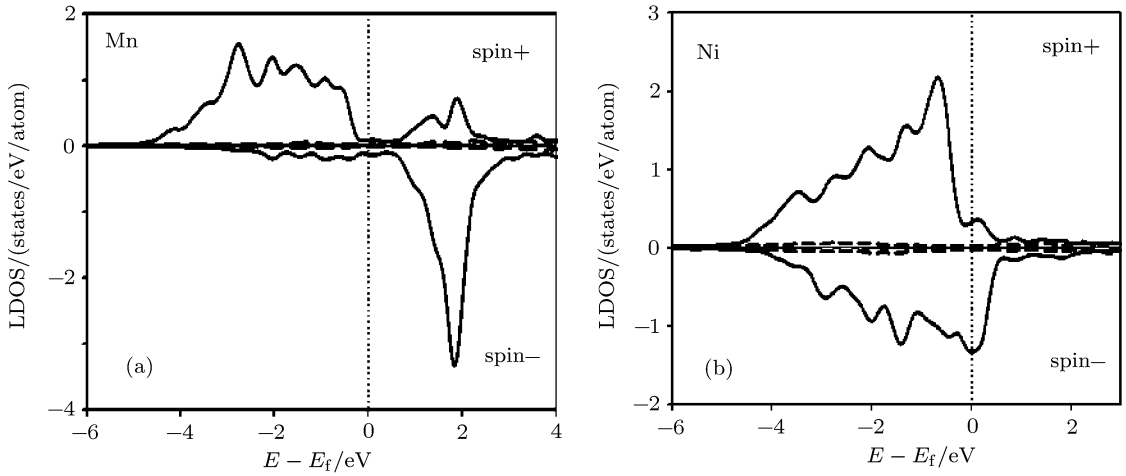


Fig. 2. Curves for spin-polarized local density of states (LDOS) for Mn–Ni(110) $c(2\times2)$, where solid and dash lines represent d-DOS and p-DOS, respectively.

Figures 3 (a) and 3(b) display the curves for the total DOS of the Ni, which is the nearest-neighbour to the Mn adatom in the Mn–Ni(110) $c(2\times2)$-sub1 and sub2, respectively, and that of the corresponding Ni atom in a Ni(110) $c(2\times2)$ vacancy structure. As can be seen from Fig. 3(a), the main peak intensities of the DOS for surface substitutional adsorption geometries with different magnetic coupling orientations are all enhanced with respect to those for the vacancy structure, meaning that the Mn adsorption on the Ni(110) $c(2\times2)$

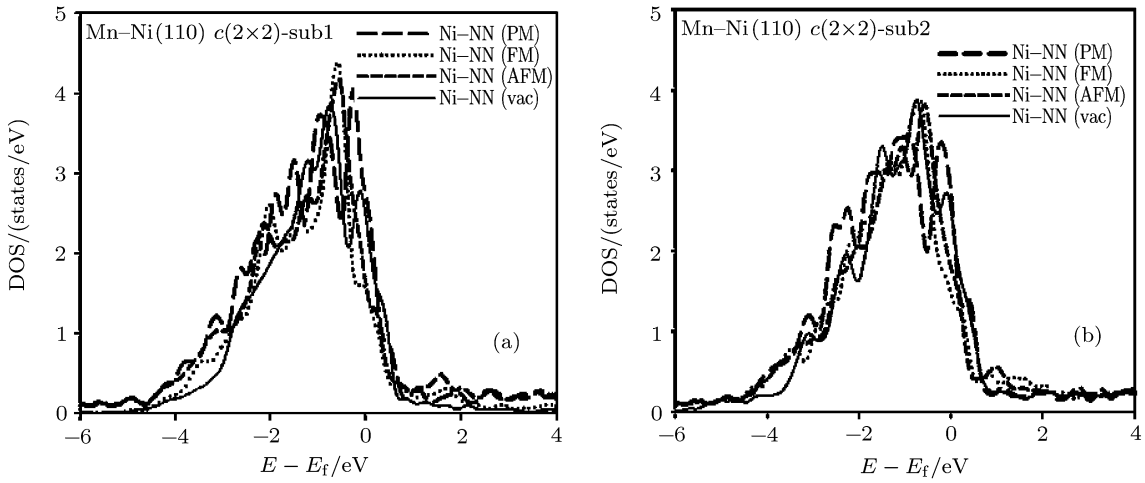


Fig. 3. Total DOS of the Ni nearest-neighbour (NN) to the Mn adatom with PM, FM and AFM couplings in (a) Mn–Ni(110) $c(2\times2)$-sub1 and (b) Mn–Ni(110) $c(2\times2)$-sub2, and that of the corresponding Ni atoms in a Ni(110) $c(2\times2)$ vacancy structure.

surface leads to charge transfer from the adsorbate to the substrate. For the DOS of the nearest neighbouring Ni atoms in the FM configuration, the peaks occur at around 1.7 eV and –2 eV and locate at nearly the same energy levels as that of the centre of mass of Mn–3d minority- and majority-spin states. These results further confirmed the strong hybridization of Mn–3d with Ni–3d orbitals. Figure 3(b) shows that the main peak intensities of the DOS for the nearest Ni neighbour to the Mn atoms with FM and AFM coupling in the subsurface layer are almost identical to those for vacancy structures, and the peak strength of DOS for the PM coupling case is slightly weaker, but its width becomes broadened. This may indicate that there is almost no charge transfer for the substitutional adsorption in the subsurface layer.

In order to further investigate the nature of the interaction between Mn adsorbate and Ni substrate, we performed the DOS analysis for the FM surface at different Mn coverages as shown in Fig. 4. The centre of mass of the minority and majority Mn bands shift upward in energy with coverage increasing, and the larger exchange splitting leads to a higher magnetic moment of the Mn atom. These results are consistent with those of Co adsorption on Cu(001) surface.[4]

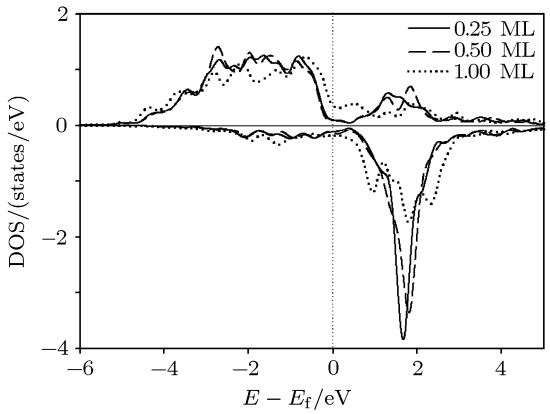


Fig. 4. Curves for total DOS for 0.25 ML (solid line), 0.5 ML (dash line), and 1.0 ML (dot line) Mn adsorbed on Ni(110) surface.

We have also estimated the Mn-induced work-function change $\Delta\Phi$ of the Ni(110) $c(2\times2)$ phase, which is defined as $\Delta\Phi = \Phi_{\mathrm{Mn-substrate}} - \Phi_{\mathrm{substrate}}$, where $\Phi_{\mathrm{Mn-substrate}}$ and $\Phi_{\mathrm{substrate}}$ are the work-function of the system with and without Mn adsorbate, respectively. $\Phi_{\mathrm{substrate}}$ is calculated to be 4.62 eV with the spin-polarized surface, which is well consistent with the earlier theoretical results of 4.55 eV[23] and 4.60 eV.[24] Without considering the spin-polarization effect, $\Phi_{\mathrm{substrate}}$ of the bare surface is obtained to be 4.69 eV. The calculated work-function changes due to Mn adsorption are shown in Table 2. For the most stable structure of substitutional adsorption in the top layer with the FM surface, $\Delta\Phi$ is estimated to be –0.59 eV, which suggests that partial charges are transferred from the Mn adsorbate to the Ni substrate. Such a phenomenon may be caused by the fact that the electronegativity of Mn is lower than that of Ni, which leads to the electron transfer to the substrate layer, and the adatom valence charges become polarized towards the substrate. Subsequently a positive dipole is formed and the work-function is decreased.[25] We also find that the work-function change value for the Mn–Ni(110) $c(2\times2)$ surface alloy is very close to that for the Mn–Ni(100) $c(2\times2)$ structure ($\Delta\Phi$: –0.52 eV).[8] In the case of substitutional adsorption in the top layer with different magnetic surfaces, the work-function change follows the trend of FM>AFM>PM, consistent with different intensities of the main DOS peaks shown in Fig. 3(a). For the substitutional adsorption in the subsurface layer, the work functions are nearly the same for the different magnetic surfaces, and no charge transfer occurs. Besides, the work-function for the ferromagnetic surface alloy decreases more significantly than that for the paramagnetic configuration. The large modification of the electronic structure, which causes the work-function change, may arise from the high magnetic moments of Mn atoms.

Table 2. Mn-induced work-function change of the Ni(110) $c(2\times2)$ phase with FM, AFM and PM surfaces. $\Delta\Phi$ refers to the work-function change.

	FM			AFM			PM		
	sub1	sub2	hol	sub1	sub2	hol	sub1	sub2	hol
$\Delta\Phi$/eV	–0.59	–0.06	–0.58	–0.52	–0.04	–0.98	–0.22	0.09	–0.69

3.3. Magnetic properties

The adsorption energies calculated for the different structural models show that the FM and the AFM Mn/Ni surface alloys are always more favourable than the PM system. From Table 1, we can see that the

energy gain in the case of on-surface adsorption due to spin polarization is stronger than that for the case of substitutional adsorption, which may be attributed to the fact that the lower coordination of the adsorbate on the surface results in a stronger localization of Mn–3d state and subsequently a larger gain in magnetic energy. Our results also suggest that the substitutional alloy in the top layer is the preferred structure when the spin polarization is considered. However, for the PM surface, the substitutional alloy in the subsurface layer is the most stable. Hence, it can be concluded that the magnetism can stabilize the surface alloy and change the stable phase of the Mn/Ni alloy.

For various combinations of AFM coupling for Mn adsorption on the Ni(110) (2×2) surface, we performed a series of calculations including the $c(2\times2)$ and the $p(2\times2)$ phases as shown in Fig. 5. We found that the substrate Ni–Ni atoms are always ferromagnetic interaction and the $c(2\times2)$ phase is more stable than the $p(2\times2)$ phase. The adsorption energy calculations show that the most stable configuration is the AFM coupling between the Mn adatoms with the $c(2\times2)$ phase as listed in Fig. 5(a). On the other hand, the adsorption energy of the most stable configuration for the AFM coupling is 0.2 eV higher than that for the FM coupling system. The results indicate that for the system of 0.5-ML Mn adsorption on the Ni(110) surface, the Mn atoms and the Ni atoms are ferromagnetic order and their magnetization directions are parallel to each other, which is in accordance with results from Mn 2P x-ray absorption spectroscopy.[10]

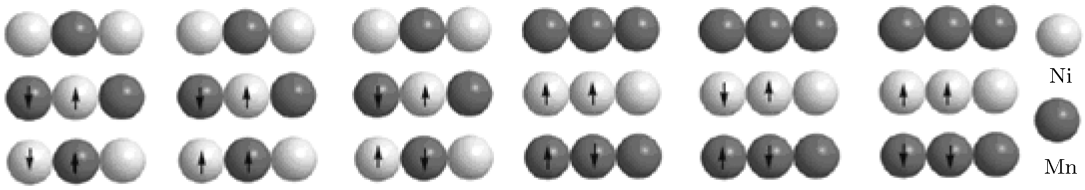


Fig. 5. Different configurations of AFM coupling for Mn adsorption on the Ni(110) surface. The arrow directions indicate the spin-up and spin-down of magnetic moment.

On the other hand, the noncollinear magnetism due to spin–orbit coupling was also discussed. The results show that it is weak in this system. It may be explained by the fact that the Mn atom has a half-filled d-shell. In addition, Nonas *et al.*[26] have studied the magnetocrystalline anisotropy energy (MAE) of Mn adsorption on Ag surfaces which have a strong spin–orbit couplings, and found that the MAE is less than 5 meV. Therefore, for Mn adsorption on Ni surface, the MAE should be weaker.

3.4. Comparison with similar adsorption systems

Our calculations have suggested that the Mn–Ni(110) $c(2\times2)$ is a magnetic surface alloy and the magnetism of Mn affects the surface structures and electronic properties significantly. Such a phenomenon has also been observed for other magnetic alloys. Table 3 lists some main parameters for Mn/Ni and Mn/Cu surface alloys. We find that all the surface alloys have large bucklings due to high magnetic moment of Mn and the magnetic moments of Mn decrease in the order of (110)>(100)>(111), corresponding to coordination decrease in the same order. It is predicted that the magnetic moment of Mn for Mn–Ni(111) $c(2\times2)$ surface alloy is smaller than 3.5 $\mu_{\rm B}$. The buckling of Cu-based surface alloys decreases in the following order: (111)>(100)>(110), consistent with the trend of the vacancy formation energy, but different from that of magnetic moment. In the case of Ni–based surface alloy, the buckling of Mn–Ni(110) $c(2\times2)$ is larger than that of Mn–Ni(100) $c(2\times2)$ surface alloy, which may be described by the magneto-volume effect, but not follow the trend of the vacancy formation energy. Hence, we suggest that the buckling of magnetic surface alloy is affected by the magnetisms of both adsorbate and substrate, and also by the vacancy formation energies of the different surfaces. Also, the magnetism of Ni is responsible for the difference in buckling order between Ni–based surface alloy and Cu-based surface alloy. On the other hand, the buckling of Mn–Ni(110) $c(2\times2)$ surface alloy is larger than that of Mn–Cu(110) $c(2\times2)$ system in spite of their almost identical magnetic moments of Mn atoms. This can be explained by simple geometrical effects that the Ni–Ni interatomic distances are 3%

shorter than Cu–Cu distances in the bulk. However, the same trend has not been observed for Mn–Ni(100) $c(2\times2)$ and Mn–Cu(100) $c(2\times2)$ surface alloys. The reason for this is that the geometrical effect of the (110) surface is dominantly responsible for the difference in buckling among different substrates when the magnetic moment difference is only 0.01 $\mu_{\rm B}$, while the difference in buckling among the (100)-oriented surface alloys mainly occurs from the magneto-volume effect due to the large magnetic moment difference (0.25 $\mu_{\rm B}$). Similar to the magnetic moment change trend, the work-function change decreases in the same order: (110)>(100)>(111).

Table 3. Comparison of some main parameters between Mn–Ni(110) $c(2\times2)$ alloy and some other alloys with similar structures: Mn–Ni(100) $c(2\times2)$, Mn–Cu(110) $c(2\times2)$, Mn–Cu(100) $c(2\times2)$, Mn–Cu(111) $c(2\times2)$. Expt. denotes experimental results, theor. represents theoretical results, and $E_{\rm f}$ refers to vacancy formation energy.

	Ni(110)	Ni(100)	Cu(110)	Cu(100)	Cu(111)
ΔZ_1/Å (Expt.)	0.30[9]	0.25[27]	0.22[17]	0.30[27,6]	
ΔZ_1/Å (theor.)	0.26	0.20[18]	0.16[17]	0.24[6]	0.29[19]
$\mu_{\rm Mn}/\mu_{\rm B}$ (theor.)	3.81	3.5[8]	3.82[17]	3.75[8]	3.59[19]
$\Delta\Phi$/eV (theor.)	–0.59	–0.52[8]	–0.48[17]	–0.31[8]	–0.18[19]
$E_{\rm f}$/eV (theor.)	0.48	0.63[16]	0.25[28]	0.43[28]	0.71[28]

4. Summary

The DFT–GGA method is used to study Mn adsorption on Ni(110) $c(2\times2)$ surface, and PM, FM and AFM surfaces both in the top layer and in the second layer are considered. It is found that substitutional alloy in the outermost layer with FM surface is the most stable in all the cases, and substitutional alloy in the subsurface layer is preferred provided that only PM configuration is considered. It is proved that the magnetism of Mn can stabilize this surface alloy due to an increase in magnetic energy. The buckling of the top layer of the Mn–Ni(110) $c(2\times2)$ surface alloy is 0.26 Å (1 Å=0.1 nm) and the rippling of the third layer is only 0.038 Å, consistent well with the experimental results. The DOS analysis shows a large magnetic splitting for the Mn atom which is slightly higher than that of Mn–Ni(100) $c(2\times2)$ surface alloy (3.41 eV) due to the higher magnetic moment. A strong hybridization between 3d states of Mn and Ni is also observed. The work-function change due to Mn adsorption is found to be –0.59 eV, and charge transfer from the adsorbate to the substrate is confirmed. The magnetic moment of Mn atom is calculated to be 3.81 $\mu_{\rm B}$. The large magnetic moment of Mn is responsible for both the large buckling of the surface alloy and the work-function change. Also, the comparison between our results and those from similar adsorption systems suggests that the buckling of the magnetic surface alloy is affected by the geometrical effect, magneto-volume effect and the vacancy formation energy.

References

[1] Kim W, Oh S J, Seo J, Kim J S, Min H G and Hong S C 1998 *Phys. Rev.* B **57** 8823

[2] Dennler S and Hafner J 2005 *Phys. Rev.* B **72** 214413

[3] Schieffer P, Krembel C, Hanf M C, Gewinner G and Gauthier Y 2002 *Phys. Rev.* B **65** 235427

[4] Pentcheva R and Scheffler M 2002 *Phys. Rev.* B **65** 155418

[5] Bode M, Heinze S, Kubetzka A, Pietzsch O, Hennefarth M, Getzlaff M, Wiesendanger R, Nie X, Bihlmayer G and Blügel S 2002 *Phys. Rev.* B **66** 14425

[6] Wuttig M, Gauthier Y and Blügel S 1993 *Phys. Rev. Lett.* **70** 3619

[7] O'Brien W L and Tonner B P 1995 *Phys. Rev.* B **51** 617

[8] Rader O, Gudat W, Carbone C, Vescovo E, Blügel S, Kläsges R, Eberhardt W, Wuttig M, Redinger J and Himpsel F J 1997 *Phys. Rev.* B **55** 5404

[9] Rader O, Mizokawa T, Fujimori A and Kimura A 2001 *Phys. Rev.* B **64** 165414

[10] Xie T, Kimura A, Kanbe T, Qiao S, Muro T, Taniguchi M, Imada S and Suga S 2003 *Jpn. J. Appl. Phys.* **42** 4695

[11] Santis M De, Abad-Langlais V, Gauthier Y and Dolle P 2004 *Phys. Rev.* B **69** 115430

[12] Kresse G and Joubert J 1999 *Phys. Rev.* B **59** 1758

[13] Perdew J P, Chevary J P, Vosko S H, Jackson K A, Pederson M R, Singh D J and Fiolhais C 1992 *Phys. Rev.* B **46** 6671

[14] White J A and Bird D M 1994 *Phys. Rev.* B **50** 4954

[15] Neugebauer J and Scheffler M 1992 *Phys. Rev.* B **46** 16067

[16] Li D F, Xiao H Y, Zu X T and Dong H N 2007 *Mater. Sci. Eng.* A **460-461** 50

[17] Ross Ch, Schirmer B, Wuttig M, Gauthier Y, Bihlmayer G and Blügel S 1998 *Phys. Rev.* B **57** 2607

[18] Bihlmayer G, Asada T, Abt R and Blügel S 2000 *Proc. International Symposium on Structure and Dynamics of Heterogeneous Systems* (Singapore: World Scientific) p. 179

[19] Bihlmayer G, Kurz Ph and Blügel S 2000 *Phys. Rev.* B **62** 4726

[20] Villars P and Calvert L D 1991 *Pearson's Handbook of Crystallographic Data for Intermetallic Phases* (Ohio: American Society for Metals, Materials Park)

[21] Quinn P D, Bittencourt C, Brown D, Woodruff D P, Noakes T C Q and Bailey P 2002 *J. Phys.: Condens. Matter* **14** 665

[22] Spisak D and Hafner J 1999 *J. Phys.: Condens. Matter* **11** 6359

[23] Kresse G and Hafner J 2000 *Surf. Sci.* **459** 287

[24] Mittendorfer F, Eichler A and Hafner J 1999 *Surf. Sci.* **423** 1

[25] Keung T C, Kao C L, Su W S, Feng Y J and Chan C T 2003 *Phys. Rev.* B **68** 195408

[26] Nonas B, Cabria I, Zeller R, Dederichs P H, Huhne T and Ebert H 2001 *Phys. Rev. Lett.* **86** 2146

[27] Wuttig M, Knight C C, Flores T and Gauthier Y 1993 *Surf. Sci.* **292** 189

[28] Xiao H Y, Zu X T, He X and Gao F 2006 *Chem. Phys.* **325** 519